NANO LETTERS

2005
Vol. 5, No. 6
1117−1122

High Rectifying Efficiencies of Microtubule Motility on Kinesin-Coated Gold Nanostructures

Martin G. L. van den Heuvel,[†] Christopher T. Butcher,[†] Ralph M. M. Smeets,[†] Stefan Diez,[‡] and Cees Dekker*,[†]

Kavli Institute of Nanoscience, Section Molecular Biophysics, Delft University of Technology, Lorentzweg 1, 2628 CJ Delft, The Netherlands, and Max Planck Institute of Molecular Cell Biology and Genetics, Pfotenhauerstrasse 108, 01307 Dresden, Germany

Received April 8, 2005; Revised Manuscript Received April 25, 2005

ABSTRACT

We demonstrate highly efficient rectification of microtubule motility on gold nanofabricated structures. First, we present a novel nanofabrication process for the creation of gold tracks for microtubule motility recessed in silicon oxide. This approach is particularly useful because it enables the use of the well-understood PEG–silane chemistry on SiO_2 for the blocking of kinesin, whereas the gold tracks allow possible electrical control. We demonstrate excellent confinement of microtubule motility to the gold nanostructures and that microtubules move on the gold with speeds comparable to that on glass. Second, we present designs of three advanced rectifier geometries. We analyze the microtubule pathways through the geometries, and we demonstrate highly efficient rectification with up to 92% efficiency. As a result, we find that up to 97% of the microtubules move unidirectionally.

Introduction. Biomolecular motors are complex nanosized protein assemblies that have the ability to convert chemical energy into mechanical work. The motor protein kinesin uses the energy from ATP hydrolysis to step along microtubule filaments.[1] A microtubule is a protein assembly, consisting of tubulin subunits polymerized into a tubular structure with an outer diameter of 25 nm and lengths up to tens of micrometers. Integration of biomolecular motors in nano-engineered environments may lead to new technologies in which parallel and automated control of molecular matter may become possible.[2] In the inverted gliding assay, kinesin motor proteins are adsorbed onto a substrate, and microtubules are propelled in random directions over the surface. If the kinesin−microtubule system is to be used in a reliable transportation system, then the movement of microtubules has to be effectively guided, confined, and directed. In particular, the rectification of microtubule movement will be crucial for molecular sorting applications, where it is envisioned that a large number of microtubules approaches a Y junction unidirectionally from one side. Efforts have been made to create micro- and nanofabricated channels in a combination with chemical patterning to confine and guide the motion of microtubules.[3−6] Unidirectional motion of microtubules in fabricated structures has been obtained by using arrow-shaped rectifier designs that redirected microtubule motion with up to 70% efficiency.[3] In all previous work, contrast in active motor density was obtained by using polymer material and absorbed detergents or block copolymers as the inactive region and glass substrates as the motility-supporting material. However, the mechanism behind the blocking of kinesin adsorption on the detergent-coated polymers is generally not well understood, and conflicting results have been reported.[3,4,7] Moreover, we previously demonstrated that the integration of metal electrodes into the structures can be advantageous, for example, to use electric fields to control microtubule docking.[8]

In this work, we describe a new fabrication process for the creation of gold tracks for microtubule motility recessed in silicon oxide (SiO_2). We show that motility is possible on gold surfaces, and we demonstrate a high contrast in microtubule motility on gold versus PEG-coated SiO_2. We present designs of three advanced rectifier geometries aimed at high rectification efficiencies. We demonstrate and analyze the highly efficient rectification in all three rectifier geometries.

Fabrication Process. To achieve a high contrast in active motor density, we use nanofabrication techniques combined with chemical adsorption (Figure 1a). As substrates, we used silicon wafers on which a 1-μm-thick layer of SiO_2 was thermally grown. The Si/SiO_2 substrates were cleaned by

* Corresponding author. E-mail: dekker@mb.tn.tudelft.nl. Fax: +31-15-2781202.
[†] Kavli Institute of Nanoscience.
[‡] Max Planck Institute of Molecular Cell Biology and Genetics.

10.1021/nl0506554 CCC: $30.25
Published on Web 05/11/2005

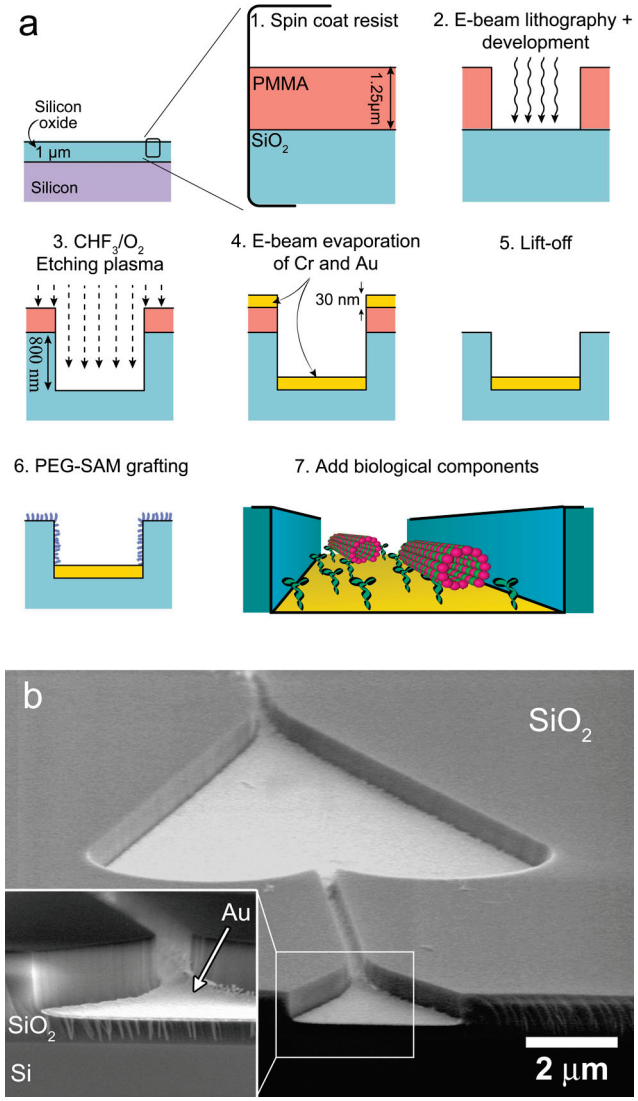

Figure 1. (a) Cross-sectional outlines of the fabrication process. Substrates are 500-μm-thick Si wafers on which a 1-μm-thick layer of SiO_2 was thermally grown. In the first step, an e-beam-sensitive resist layer was spin-coated onto the substrates. Then, e-beam lithography was used to define the structures, and the pattern was developed. In the third step, an etching plasma transferred the patterns into the SiO_2. Then, e-beam evaporation was used to deposit 5-nm chromium and 30-nm gold. Fifth, lift-off was done to remove the resist and metal layers outside of the trench bottoms. In the sixth step, a PEG monolayer (~3-nm tail size) was grafted onto the SiO_2 to block motility outside the gold areas. Finally, kinesin was adsorbed onto the gold, and the microtubules move through the trenches. (b) SEM image of a rectifier structure. The substrate was broken to show the device in cross section. SEM imaging was done under an angle. The inset shows 2× magnification of the cross section.

subsequent sonications during 5 min in acetone, fuming nitric acid, and 2-propanol (IPA). Then, a 1.25-μm-thick layer of electron-beam (e-beam)-sensitive resist poly(methyl methacrylate) (PMMA, molecular weight 950K, 7% solution of PMMA dissolved in chlorobenzene) was spin-coated (2250 rpm for 1 min) onto the substrate. The samples were baked on a hot plate for 15−40 min at 175 °C. Structures were written with a Leica electron-beam pattern generator with a dose of 1600 $\mu C/cm^2$. The samples were developed by a 75-s immersion in a mixture (1:3) of methyl-isobutyl ketone and IPA and a subsequent immersion of 25 s in IPA to stop the development. We then used a reactive-ion etching step in CHF_3/O_2 plasma (flow rates of 100 and 2.5 sccm) to transfer the pattern ~800 nm into the SiO_2. The dry etching creates a highly anisotropic trench profile with steep sidewalls. The pressure of the plasma was set to 50 μbar to achieve an anisotropic etch and keep the etch selectivity between the SiO_2 and PMMA reasonable. Etch rates for SiO_2 and PMMA were ~30 and 23 nm min^{-1}, respectively. e-beam evaporation was used to deposit first a 5-nm sticking layer of chromium (Cr) and then a 30-nm-thick layer of gold onto the substrates. Lift-off was performed to remove the resist such that only the metal on the bottom of the trench was left. To enhance the lift-off, we exposed the samples for 7.5 min to a high-pressure (200 μbar) O_2 (50 sccm) plasma etch. The lift-off was done by sonicating the samples for 2 min in heated (90 °C) positive-resist stripper (PRS3000), sonicating for 10 s in ddH_2O, and sonicating for 10 s in IPA.

To block motility on the trench sidewalls and elevated SiO_2 regions, we used a poly(ethylene glycol) (PEG) self-assembled monolayer (SAM) that is known to be protein-repellant.[9,10] The grafting of the PEG-SAM was based on the protocol described in ref 9. The trimethoxysilane headgroup of the SAM covalently binds to the SiO_2 such that the PEG tails stick out from the surface. The samples were first sonicated for 5 min in a mixture of ethanol and water (1:1). Then the samples were submersed for 10 min in Piranha solution, a strongly oxidating mixture of hydrogen peroxide (31%) and sulfuric acid (96%) in a 3:1 mixture, heated to 75 °C. Then the samples were rinsed three times in ddH_2O and once in ethanol and finally sonicated for 10 min in ddH_2O. After sonication, the samples were blown dry with nitrogen and directly immersed in the PEG solution. The PEG solution consisted of 5 mM 2-[methoxypoly(ethyleneoxy)propyl]-trimethoxysilane (90%, ABCR Karlsruhe, molecules about 3 nm long) and 0.08%$_v$ hydrochloric acid (36%) in toluene. After 24 h, the samples were taken out of the grafting solution, rinsed in toluene, rinsed in ethanol twice, rinsed in ddH_2O twice, sonicated in ddH_2O for 2 min, and finally blown dry with nitrogen.

Device Characterization. In Figure 1b, we show a scanning electron microscope (SEM) image of a cross section of a nanofabricated structure for microtubule motility. The arrowlike structure was designed to rectify microtubule motility as discussed below. The picture clearly shows recessed areas covered with gold and elevated SiO_2 plateaus. The inset shows a close up of the cross section, where the boundary between the Si and the thermally grown SiO_2 layer is clearly visible. The trenches have a rectangular profile as a result of the dry etching. Because of the rectangular profile and the fact that e-beam evaporation is a very directional process, the gold is evaporated only on the trench bottoms and not on the trench sidewalls. In combination with the PEG grafting on the SiO_2, this prevents kinesin molecules from adsorbing onto the trench sidewalls and accordingly helps to confine the microtubules to the trenches.

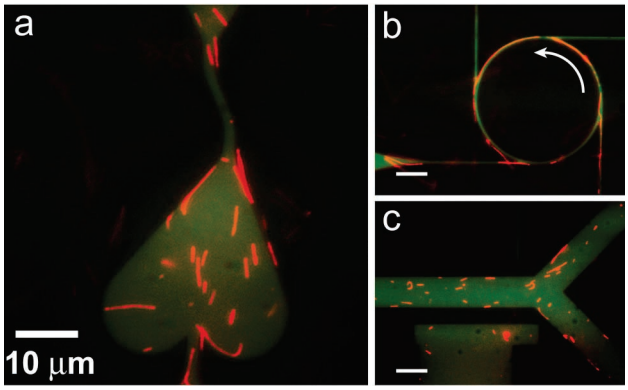

Figure 2. Overlay images of a bright field picture of the gold structures (green) and fluorescence images of microtubules (red). All images show a very clear contrast in microtubule density between the gold and SiO_2 areas (black). All scale bars are 10 μm. (a) Rectifier structure. The Supporting Information shows a movie of microtubule motility in such a structure. (b) Circular structure used to generate motility in the counterclockwise direction. (c) Straight track ending in a Y junction.

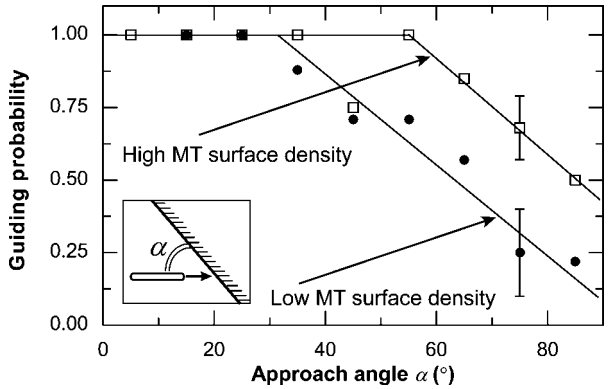

Figure 3. Guiding probability of a microtubule after sidewall collisions under different angles (inset). Microtubules moving through a rectifier structure were traced, and the approach angle and outcome were recorded for each collision. Results were collected in 10° bins. The black open squares show the data (98 events) for a motility assay with a high microtubule surface density; gray dots show the results (60 events) for an assay with a low microtubule surface density. Lines are guides to the eye. Standard errors shown are typical for the data.

Motility Characterization. We tested microtubule motility[11] in our nanofabricated structures using a flow cell constructed from the substrate, spacers of double-sided tape, and a microscope glass cover slip. The microtubules were imaged by fluorescence microscopy on an inverted Olympus IX81 microscope using a Zeiss 100X oil-immersion objective (1.30 NA) and a Hamamatsu Orca CCD camera.

Figure 2 shows images of a high contrast in microtubule motility in three different structures. Figure 2a shows a rectifier structure intended to redirect the downward motion of microtubules into the upward direction.[3] Figure 2b shows a circular track with four straight tangential connections, which causes microtubules to move in the counterclockwise direction.[12] In Figure 2c, we show a track ending in a Y junction. In each picture, we superimposed a bright-field reflection image of the gold−SiO_2 substrate (green) with a fluorescence image (red) of the microtubules.

We find a clear contrast in the density of microtubules between the gold and the PEG-coated SiO_2. Microtubules are observed to move only on the recessed gold areas but never on the SiO_2 plateaus. In the same experiments, however, motility was always observed on the glass cover slip. In control experiments with the PEG−SAM omitted, microtubules moved over both the gold and the SiO_2 regions (data not shown). We attribute the absence of motility on the SiO_2 to a low concentration of kinesin molecules due to the protein repellant properties of the PEG.[10] We determined that microtubules moved on the gold with a speed of 0.73 ± 0.13 μm s^{-1} (mean ± standard deviation). This compares well with the speed on the glass cover slide (0.78 ± 0.08 μm s^{-1}).

We observe a distinct variation in the microtubule density on the gold nanostructures from different experiments. Under similar experimental conditions, some samples show a microtubule surface density that is comparable to that on the glass cover slip as well as good guiding within the channels, whereas other samples had almost no microtubules moving over the gold and a high chance of microtubule detachment upon colliding with sidewalls. These differences were not due to the fabrication process or chemical surface treatments because we also observed the variations between samples that were prepared in the same run. To quantify these observations, we examined the guiding probability for microtubules upon colliding with sidewalls in our structures. To this aim, we traced microtubules moving through a rectifier structure, and we measured, for each collision with a sidewall, the approach angle (α) and the outcome of the collision (guided along the wall and remaining on the surface or detached from the gold and lost to solution). Figure 3 shows the guiding probability as a function of approach angle (in 10° bins) for two typical assays. The assay with high microtubule surface density shows very effective guiding (100%) up to collision angles of 50−60°. Only for higher angles does the probability of staying within the channel decrease to about 50% for orthogonal collisions. The assay with a low microtubule surface density already shows a decrease in guiding probability for angles higher than 20−30°, and the probability drops to about 20% for orthogonal collisions. The guiding performance for high collision angles in our devices is less than in some reports by other groups,[4,5] who used resist sidewalls on glass substrates. This may be due to a lower kinesin density on gold compared to that on glass surfaces.[8] The method presented in this work has the advantage of integrating metal electrodes into the tracks.

A variation in the active kinesin density is a possible explanation for the decreased guiding performance at high collision angles and the varying microtubule density among samples. The equilibrium surface density of microtubules is proportional to the bulk microtubule concentration and the binding affinity (defined as the on rate divided by the off rate) of microtubules.[8] The bulk concentration of microtubules is approximately constant between different experiments. Furthermore, possible differences in the microtubule concentration would not affect the guiding probability (Figure 3). However, we expect that a lower motor density has a

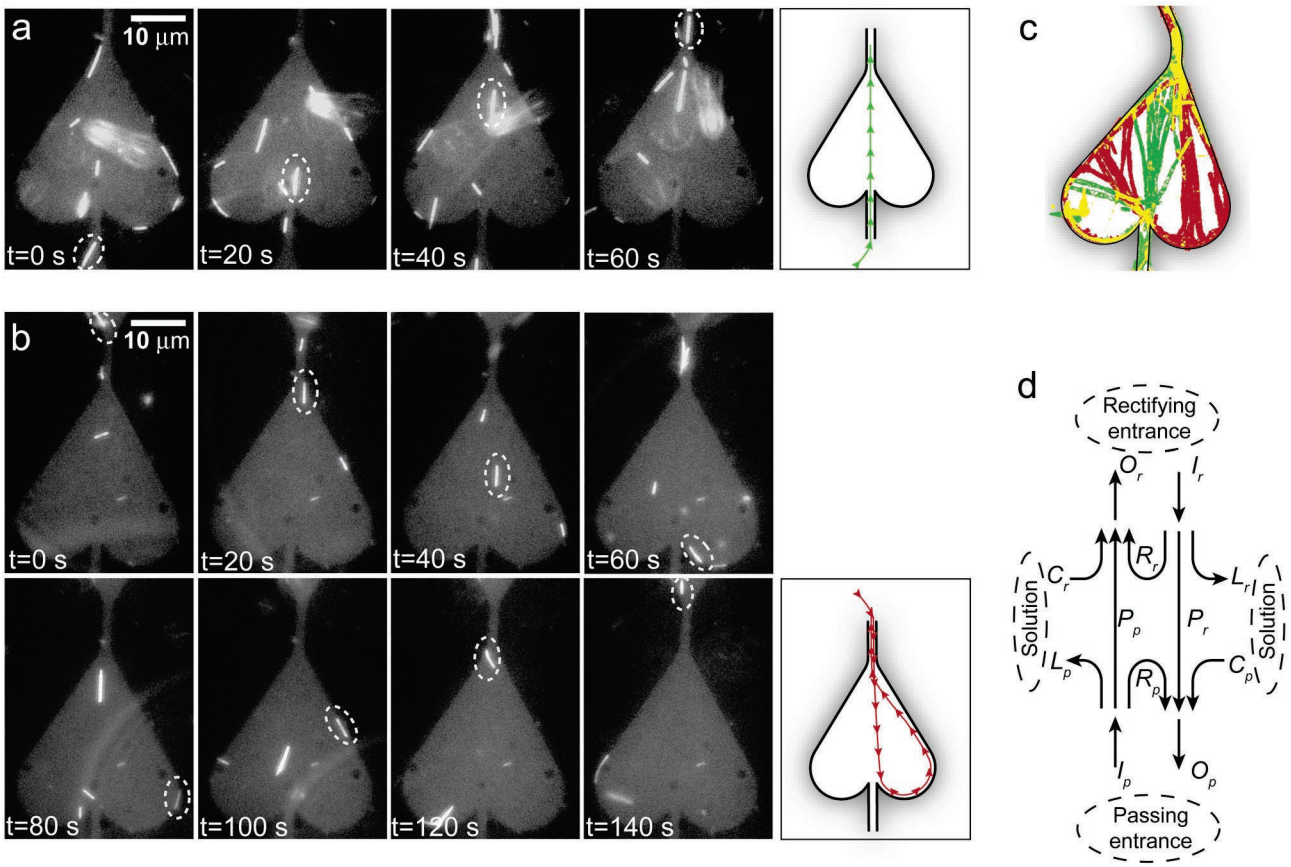

Figure 4. Microtubule traversal through a rectifier structure. The structure is designed to rectify microtubule motility in the upward direction. Microtubules entering the structure from below should pass unhindered. (a) Demonstration of a passing event. A microtubule entering the structure from below traverses the structure in 60 s and exits through the upper channel. The picture on the right traces the traversed path. (b) Demonstration of a rectification event. A microtubule entering the structure from the upper channel at $t = 0$ s traverses the structure, collides with the round region at the right side at $t = 60$ s, and is redirected along the sidewalls ($t = 80$, 100, and 120 s) in the upward direction. Finally ($t = 140$ s), it exits the structure through the same channel. As a result of the process, its velocity has been reversed. The picture on the right traces the traversed path. (c) Overlay image of all microtubule paths that were traversed during 75 s in a rectifier of design B. Microtubule paths originating from the upper entrance are shown red, and microtubules from the lower entrance are shown green. The yellow areas result from overlapping green and red traces. (d) Schematic classification of all possible pathways of microtubules traversing a rectifier structure. Arrows denote the direction of motion. Symbols are defined in the text and represent numbers of microtubules.

negative effect on both the binding affinity and the guiding probability. We thus speculate that the kinesin density varies among different samples for reasons that are so far not well understood.

Rectification of Motility. To demonstrate and achieve unidirectional motion of randomly moving microtubules, we designed and tested three different rectifier geometries. The designs with relevant dimensions are shown in Figure 5b–d. The rectifiers are all designed to rectify microtubule motility into the upward (as drawn) direction; that is, microtubules entering from the upper channel entrance should be reversed in direction and exit through the same upper channel exit. Microtubules that enter from the lower entrance should pass through the structure and exit through the upper channel exit. Design A (Figure 5b) is the simplest form of a rectifier structure. Design B (Figure 5c) has an entrance that is slightly offset with respect to the exit to minimize the chance of a microtubule passing straight from the upper to lower channel. Finally, design C (Figure 5d) has been proposed before for a "thermal-ratchet sorting"[12,13] of the microtubules. A microtubule entering from the upper entrance has only a slight chance of making a sharp turn and passing through in the downward direction. Indeed, it has a high chance of being guided into the rounded region and being redirected toward the upper exit. The curved channels in designs B and C are meant to align the exit and entrance channels for an easy modular integration into larger designs.

Figure 4 shows examples of rectification and passing events of microtubules. Figure 4a displays snapshots with 20 s intervals of a microtubule entering from the lower entrance and exiting through the upper channel as intended. Figure 4b shows snapshots of the successful rectification of a microtubule that enters and exits through the upper entrance. At $t = 60$ s, the microtubule has collided with the sidewall at the bottom of the rounded region on the right and is being redirected by the wall ($t = 80$, 100, and 120 s) back toward the upper channel ($t = 140$ s). Figure 4c shows the superimposed traces of all microtubule paths passing through a structure of design B during 75 s. Most microtubules originating from the upper entrance (traces colored red) follow a more or less straight path down, are guided in the rounded region on the right, and are redirected by the rounded

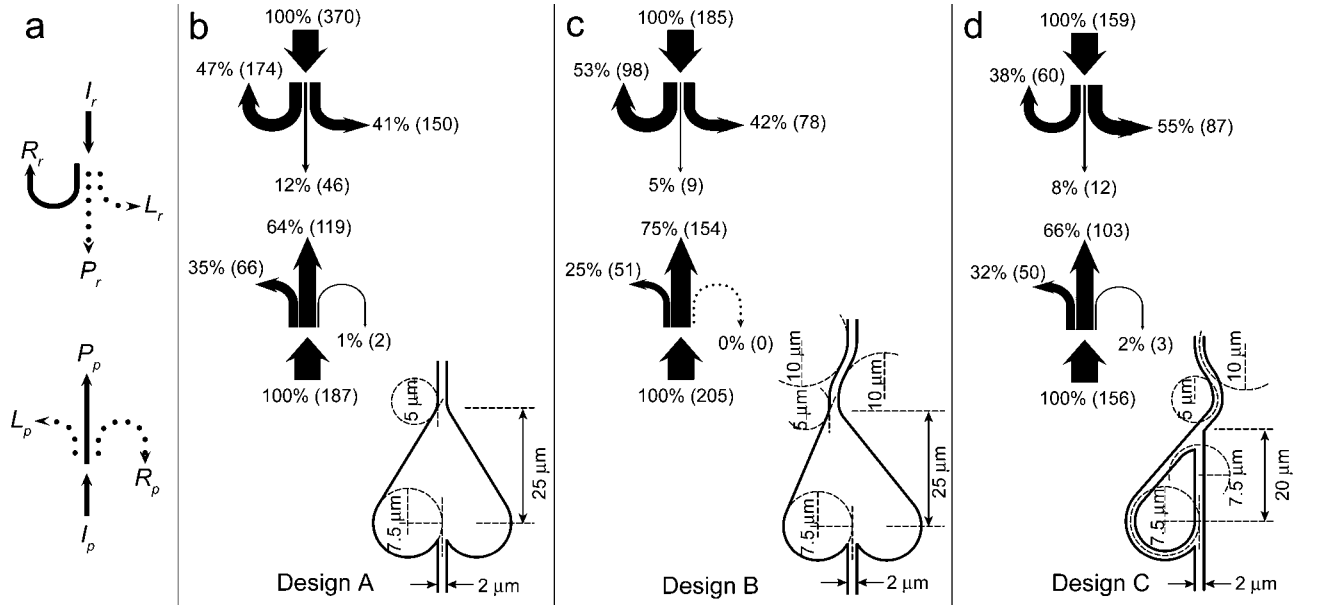

Figure 5. Results of the analysis of microtubule traversal through three different rectifier designs. (a) Legend for b−d. Desired pathways are shown by solid lines, and undesired pathways are shown by dotted lines. The rectifier geometries are designed such that microtubules entering the structure from the upper channel (I_r) should be rectified and exit through the same channel (R_r). Passing through and exiting through the other channel (P_r) or detachment and loss to solution (L_r) are undesired. Conversely, microtubules entering through the lower channel (I_p) should pass unhindered and exit through the opposite channel (P_p), whereas none should be lost (L_p) or reversed (R_p). (b−d) Results for three different designs. The arrow diagrams denote the fraction of microtubules and the absolute number (between brackets) that traverse the structure according to the legend in a. The width of the arrow scales with the fraction of microtubules. The designs with their relevant dimensions are shown on the bottom of each graph.

walls, following the sidewalls back to the original entrance. The set of microtubules that originates from the lower channel (traces colored green) mainly passes straight through the structure toward the funnel at the upper channel as intended. The yellow traces result from overlap in green and red microtubule paths.

To quantify the performance of the three rectifier designs, we systematically traced and analyzed the traversal of microtubules through the structures according to their origin and destination. As indicated in Figure 4d, microtubules can enter the structure through the lower ("passing") channel entrance (I_p) and then either be rectified (R_p), pass through the structure (P_p), or be lost to solution (L_p). Microtubules that exit the structure through the lower passing exit (O_p) have originated either from the passing entrance itself via a rectification event (R_p), from the upper ("rectifying") entrance via a passing event (P_r), or from solution via binding (C_p). A similar classification can also be made for the upper rectifying entrance by interchanging the subscripts *r* and *p*.

We demonstrate a clear asymmetry between both entrances in the number of microtubules traversing the different pathways, as shown in Figure 5. Figure 5a depicts the desired traversals in solid lines and undesired pathways in dotted lines. Microtubules entering the structure from the lower channel ought to pass through, whereas microtubules entering from the upper channel should be reversed. For the three rectifier designs, Figure 5b−d shows, for each entrance, the redirected, passed, and lost fractions (and absolute numbers) of the total number of microtubules that entered each structure. In all three designs, microtubules that enter the structure through the lower passing entrance (I_p) are mainly passed through (P_p = 64 to 75%) as desired, whereas only a negligible number of microtubules are reversed (R_p = 0 to 2%). The remainder of the microtubules is lost to solution, mainly after collisions with sidewalls. Conversely, of the microtubules entering through the upper rectifying entrance (I_r) a large fraction reverses its direction (R_r = 38 to 53%) as intended, and only a small fraction passes through without being rectified (P_r = 5 to 12%). The remainder of the microtubules is lost to solution. The observed losses are roughly consistent with the data presented in Figure 3 for high collision angles. It is difficult to distinguish between the rectifying efficiencies of the three different designs by a straightforward comparison of the R_r values because the variation in the fraction of microtubules that is lost to solution (L_r varies between 41 and 55%) is about as large as the variation in R_r (between 38 and 53%), obscuring possible differences in the rectifying efficiencies.

To enable a meaningful comparison between the three designs, we estimate the rectifying efficiency (η_r) and passing efficiency (η_p) with respect to the number of microtubules that remain surface-bound:

$$\eta_r = \frac{R_r}{I_r - L_r} \quad \text{and} \quad \eta_p = \frac{P_p}{I_p - L_p} \tag{1}$$

Table 1 displays the measured fractions R_r and R_p and the corresponding rectifying and passing efficiencies η_r and η_p. Excellent rectifying behavior is obtained. In all cases, the estimated rectifying efficiencies (between 0.79 and 0.92) are very high, and the passing efficiencies are close to unity.

Table 1. Measured Rectifying (R_r) and Passing (P_p) Fractions and Rectifying (η_r) and Passing (η_p) Efficiencies for Three Rectifier Designs[a]

	measured fractions		estimated efficiencies	
	R_r	P_p	η_r	η_p
design A	0.47 ± 0.03	0.64 ± 0.04	0.79 ± 0.03	0.98 ± 0.01
design B	0.53 ± 0.04	0.75 ± 0.03	0.92 ± 0.03	1.00
design C	0.38 ± 0.04	0.66 ± 0.04	0.83 ± 0.04	0.97 ± 0.02

[a] The standard errors are calculated as $\sqrt{p(1-p)/n}$.[14]

Hiratsuka et al. previously published a rectifying probability of 0.7.[3] We do not find a significant difference in the performance of the three devices, although design B seems slightly more efficient with a rectifying efficiency of 0.92 and a passing efficiency of 1.00.

As a result of the efficient rectifier geometries, we observe that a very large fraction of the microtubules traversing the lower channel move unidirectionally into the upward direction. The number of microtubules that pass through the lower channel in the upward direction is I_p, whereas the number of microtubules traversing the same channel in the downward direction is $P_r + R_p$ (Figure 5a). We thus find that in design B 97% of the microtubules in the lower channel move unidirectionally in the upward direction. In a future exploitation of rectifier geometries, the rectifying efficiencies can even be improved by placing multiple rectifiers in series.

Conclusions. We have described a novel fabrication process for the creation of gold nanotracks for microtubule motility. We used a combination of topographic patterning and chemical adsorption to create a very high contrast in active motor density, where active kinesin adsorbs only on gold patterns recessed in SiO_2 trenches. This fabrication approach offers the opportunity of using the well-understood PEG−silane chemistry to block kinesin adsorption on SiO_2, whereas the gold nanostructures can be advantageous for electrical control. We demonstrated microtubule motility in our gold nanostructures, and we observed that microtubules moved on the gold with a speed of 0.73 ± 0.13 μm s^{-1}, which is comparable to the speed on the glass cover slide (0.78 ± 0.08 μm s^{-1}). Microtubules were never present on PEG-coated SiO_2. We characterized the guiding probability of microtubules upon sidewall collisions in our structures. Finally, we introduced three new designs for rectification structures for which we thoroughly analyzed the microtubule pathways. A rectifying efficiency as high as 92% was demonstrated, whereas the passing efficiency for microtubules moving in the desired direction was about 100%. As a result, we obtained unidirectional motion of 97% of the microtubules. The possibilities of using gold as a substrate and controlling the directionality of motility may be important for the use of biomolecular motors in novel applications such as a molecular transportation system.

Acknowledgment. This work was funded by The Netherlands Organization for Scientific Research (NWO) and the EC BIOMACH project. S.D. acknowledges support from the BMBF (grant 03N8712).

Supporting Information Available: Movie of rectifying events. This material is available free of charge via the Internet at http://pubs.acs.org.

References

(1) Svoboda, K.; Schmidt, C. F.; Schnapp, B. J.; Block, S. M. *Nature* **1993**, *365*, 721−727.
(2) Hess, H.; Vogel, V. *Rev. Mol. Biotechnol.* **2001**, *82*, 67−85.
(3) Hiratsuka, Y.; Tada, T.; Oiwa, K.; Kanayama, T.; Uyeda, T. Q. P. *Biophys. J.* **2001**, *81*, 1555−1561.
(4) Moorjani, S. G.; Jia, L.; Jackson, T. N.; Hancock, W. O. *Nano Lett.* **2003**, *3*, 633−637.
(5) Clemmens, J.; Hess, H.; Lipscomb, R.; Hanein, Y.; Bohringer, K. F.; Matzke, C. M.; Bachand, G. D.; Bunker, B. C.; Vogel, V. *Langmuir* **2003**, *19*, 10967−10974.
(6) Jia, L. L.; Moorjani, S. G.; Jackson, T. N.; Hancock, W. O. *Biomed. Microdevices* **2004**, *6*, 67−74.
(7) Hess, H.; Matzke, C. M.; Doot, R. K.; Clemmens, J.; Bachand, G. D.; Bunker, B. C.; Vogel, V. *Nano Lett.* **2003**, *3*, 1651−1655.
(8) Van den Heuvel, M. G. L.; Butcher, C. T.; Lemay, S. G.; Diez, S.; Dekker, C. *Nano Lett.* **2005**, *5*, 235−241.
(9) Papra, A.; Gadegaard, N.; Larsen, N. B. *Langmuir* **2001**, *17*, 1457−1460.
(10) Zhang, M. Q.; Desai, T.; Ferrari, M. *Biomaterials* **1998**, *19*, 953−960.
(11) The protocol for the motility experiments was as follows. The flow cell was first incubated for 5 min with a casein solution containing 0.5 mg/mL casein in BRB80 buffer (80 mM Pipes, 1 mM $MgCl_2$, 1 mM EGTA, pH 6.9). Then, kinesin was added to the flow cell (6 μg/mL full-length *Drosophila* conventional kinesin in BRB80, 0.2 mg/mL casein, 1 mM ATP) and incubated for 5 min. Finally, the flow cell contents were exchanged with motility solution containing rhodamine-labeled paclitaxel-stabilized microtubules (∼30 nM tubulin, 1 mM ATP, 1 mM $MgCl_2$, 10 μM Taxol, and anti-bleaching cocktail (20 mM D-glucose, 0.020 mg/mL glucose oxidase, 0.008 mg/mL catalase, 1% β-mercaptoethanol)) all in BRB80 buffer. Microtubules were polymerized from 10 μL of bovine brain tubulin (4 mg/mL, one rhodamine-labeled unit, three unlabeled units, Cytoskeleton, Denver, CO) in the presence of 4 mM $MgCl_2$, 1 mM GTP, and 5% DMSO in BRB80 buffer (37 °C for 60 min.). Then the microtubules were stabilized and 100× diluted in BRB80 containing 10 μM Taxol.
(12) Hess, H.; Clemmens, J.; Matzke, C. M.; Bachand, G. D.; Bunker, B. C.; Vogel, V. *Appl. Phys. A* **2002**, *75*, 309−313.
(13) Clemmens, J.; Hess, H.; Doot, R.; Matzke, C. M.; Bachand, G. D.; Vogel, V. *Lab Chip* **2004**, *4*, 83−6.
(14) The standard error for binomial distributions is defined as $\sqrt{p(1-p)/n}$, where p is the measured probability of success and n is the number of observations. This definition underestimates the standard error for values of p approaching 0 or 1.

NL0506554